# Magneto-optic Kerr effect (MOKE) simulation of a Fe-Cu superlattice

Yanzhi Zhao*
*Department of Physics, Cornell University*

In this term paper, we summarize the underlying theory and present MATLAB simulations of the magneto-optic Kerr effect (MOKE) for a Fe-Cu superlattice. We implement the MOKE simulation under two different magnetization configurations, the polar configuration (POL) and the longitudinal polarization (LON). For each magnetization configuration, we analyze the dependencies of Kerr signal magnitude and reflectivity on Fe-film thickness, superlattice repetition period, and the initial incident angle.

The magneto-optic Kerr effect (MOKE) refers to the phenomenon in which a light beam's polarization and reflectivity may change when reflected from a magnetized surface. Fig. 1 illustrates MOKE: when an initially s-polarized (or p-polarized) light beam is incident on a magnetized surface, such as a ferromagnetic medium, with an initial incident angle $\theta_i$, the reflected light beam may contain both s-polarized and p-polarized components. The polarization change depends on multiple factors including the direction of the magnetization, the incident angle, the thickness, and the Voigt magneto-optic constant of the medium, etc. MOKE has been widely applied to investigate surface magnetism, one of the examples is the magneto-optic Kerr effect microscope that enables the study of the spin dynamics and domain walls in quantum materials [1].

The theory underlying MOKE is based on explicitly solving the Maxwell equations within the medium. For a non-magnetic medium, we assume the dielectric tensor is isotropic and can be replaced by a constant. In contrast, for cubic ferromagnetic medium, the dielectric tensor is antisymmetric [2]. The dielectric tensor of the magnetic and non-magnetic medium can be written into a generic form [3, 4, 5]

$$\varepsilon = N_1^2 \begin{pmatrix} 1 & i\cos\theta Q & -i\sin\phi\sin\theta Q \\ -i\cos\theta Q & 1 & i\cos\phi\sin\theta Q \\ -i\sin\phi\sin\theta Q & -i\cos\phi\sin\theta Q & 1 \end{pmatrix}$$

Where $N_1$ is the refraction index of medium 1 (non-magnetic medium in Fig. 2(a) or magnetic film 1 in Fig. 2(b)). $\theta$ and $\phi$ denote the polar angle and the azimuthal angle of the medium 1 magnetization, as indicated in Fig. 2(b). $Q$ is the Voigt magneto-optics constant, which is roughly proportional to the saturation magnetization of medium 1 [2]. $Q$ is nonzero for a magnetic medium (such as Fe) and zero for a non-magnetic medium (such as Cu).

Considering wave $\sim e^{i(\mathbf{k}\cdot\mathbf{r}-\omega t)}$. Suppose there is no free charge and free current source, thus $\mathbf{D}=\varepsilon\mathbf{E}$, $\mathbf{B}=\mathbf{H}$. Solving the Maxwell equations inside the medium 1, $\mathbf{k}\cdot\mathbf{D}=0$, $\mathbf{k}\times\mathbf{E}=\frac{\omega}{c}\mathbf{H}$, $\mathbf{k}\cdot\mathbf{H}=0$, $\mathbf{k}\times\mathbf{H}=-\frac{\omega}{c}\mathbf{D}$, we obtain medium 1's eigenmodes, any electromagnetic waves within medium 1 can be written as a superposition of eigenmodes.

(*I*) In a nonmagnetic medium, there are two eigenmodes, as displaced in Fig. 2(a), the incident eigenmode points toward Medium f, and the reflected eigenmode points toward Medium i. In the non-magnetic medium, L-/ R-circularly polarized waves have the same refraction index.

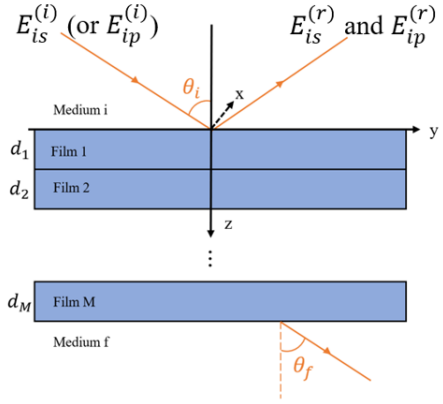


FIG. 1. Diagram of MOKE. The y-z plane is the incident plane, $E_{is}^{(i)}$ and $E_{ip}^{(i)}$ represent the initially s- and p-polarized light beam in medium i, respectively, while $E_{is}^{(r)}$ and $E_{is}^{(r)}$ denote the reflected s- and p- polarized components in medium i, respectively. Medium i is non-magnetic, and film 1 through M are ferromagnetic.

(*II*) Inside a magnetic medium, we have four eigenmodes $\bar{1}$, $\bar{2}$, $\bar{3}$ and $\bar{4}$, as displayed in Fig. 2(b). Modes $\bar{1}$ and $\bar{2}$ are incident waves (incident to the boundary between magnetic film 1 and medium f) and are R- and L-circularly polarized. Modes $\bar{3}$ and $\bar{4}$ are reflected waves (reflected from the boundary between magnetic film 1 and medium f) and are L- and R-circularly polarized. Eigenmodes $\bar{1}$, $\bar{2}$, $\bar{3}$ and $\bar{4}$ are associated with the electric field $\mathbf{E}_1^{(\bar{1},\bar{2},\bar{3},\bar{4})}$, the magnetic field $\mathbf{H}_1^{(\bar{1},\bar{2},\bar{3},\bar{4})}$, the refraction index $n_1^{(\bar{1},\bar{2},\bar{3},\bar{4})}$ and the incident angle $\theta_1^{(\bar{1},\bar{2},\bar{3},\bar{4})}$. The incident angle $\theta_1^{(\bar{1},\bar{2},\bar{3},\bar{4})}$ and the initial incident angle $\theta_i$ are related by Snell's law $N_i\sin\theta_i = n_1^{(\bar{1},\bar{2},\bar{3},\bar{4})}\sin\theta_1^{(\bar{1},\bar{2},\bar{3},\bar{4})}$, the subscript i means inside the initial medium i, and the subscript 1 means inside medium 1. In the magnetic medium, L- and R-circularly polarized waves have different refraction indexes: $n_{R,L}=N_1(1\pm\frac{1}{2}gQ)$, $g\equiv\mathbf{k}\cdot\mathbf{M}/|\mathbf{k}|\cdot|\mathbf{M}|$.

Knowing the eigenmodes, we can write down the total electromagnetic waves. To simplify the discussion, define the F-vector $F_1\equiv[E_{1x},E_{1y},H_{1x},H_{1y}]^T$ and the P-vector $P_1\equiv[E_{1s}^{(i)},E_{1p}^{(i)},E_{1s}^{(r)},E_{1p}^{(r)}]^T$. The F-vector is composed of the x- and y-components of the total electric field $\mathbf{E}_1$ and the total magnetic field $\mathbf{H}_1$ in medium 1, and the P-vector is composed of the s- and p-components of the total incident and reflected electric field ($\mathbf{E}_1^{(i)}$, $\mathbf{E}_1^{(f)}$) in medium 1. F-vector and P-vector

* yz3276@cornell.edu

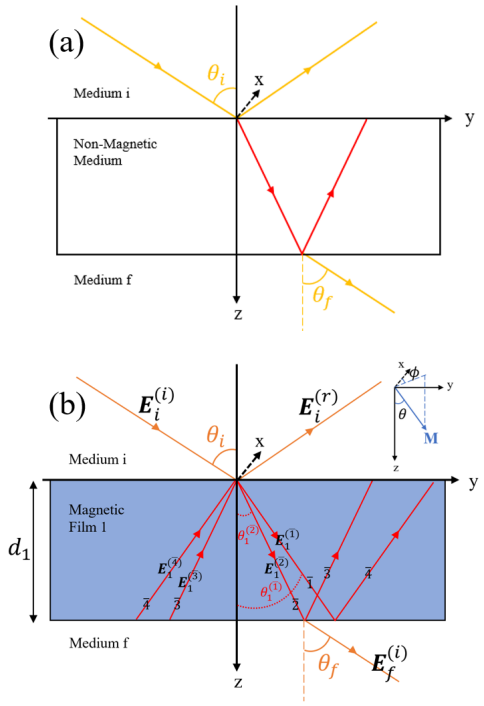


FIG. 2. Waves propagate inside (a) the non-magnetic medium and (b) the magnetic medium with thickness $d_1$. The electric field and the magnetic field are continuous across the boundary.

are related by the $4\times4$ boundary-matrix A.

$$F_1 = A_1 P_1 \tag{1}$$

When the wave propagates inside medium 1, $P_1(z=0)$ and $P_1(z=d_1)$ are linked by the $4\times4$ propagation-matrix D:

$$P_1(z=0) = D_1 P_1(z=d_1) \tag{2}$$

Ref. [4] gives the formula for boundary matrix A and propagation matrix D. The formulas are displayed in the appendix.

Since the x and y components of the electric field and the magnetic field are continuous across the boundary, we therefore have the following boundary condition: $F_i(z=0) = F_1(z=0)$, $F_1(z=d_1) = F_f(z=d_1)$. Substitute (1) and (2) into this boundary condition, we get $P_i(z=0) = \left(A_i^{-1}A_1D_1A_1^{-1}A_f\right)P_f(z=d_1)$. For multiple films, as illustrated in Fig. 1,

$$P_i(z=0) = A_i^{-1}\left(\Pi_{m=1}^{M}A_mD_mA_m^{-1}\right)A_fP_f(z=\sum_{m=1}^{M}d_m) \tag{3}$$

Define the characteristic-matrix $\mathscr{M}$,

$$\mathscr{M} \equiv A_i^{-1}\left(\Pi_{m=1}^{M}A_mD_mA_m^{-1}\right)A_f \tag{4}$$

As shown in Eq. (3), the characteristic-matrix $\mathscr{M}$ links the P-vector of the initial medium i and the P-vector of the final medium f through $P_i(z=0) = \mathscr{M}P_f(z=\sum_{m=1}^{M}d_m)$.

For an initial $s$-polarized incident beam $\mathbf{E}_{is}^{(i)}$, define the following magneto-optic coefficients: $r_{ss} \equiv E_{is}^{(r)}/E_{is}^{(i)}$, $r_{ps} \equiv E_{ip}^{(r)}/E_{is}^{(i)}$, $t_{ss} \equiv E_{fs}^{(i)}/E_{is}^{(i)}$, $t_{ps} \equiv E_{fp}^{(i)}/E_{is}^{(i)}$. For an initial $p$-polarized incident beam $\mathbf{E}_{ip}^{(i)}$, define $r_{pp} \equiv E_{ip}^{(r)}/E_{ip}^{(i)}$, $r_{sp} \equiv E_{is}^{(r)}/E_{ip}^{(i)}$, $t_{pp} \equiv E_{fp}^{(i)}/E_{ip}^{(i)}$, $t_{sp} = E_{fs}^{(i)}/E_{ip}^{(i)}$. $r_{ss,sp,ps,pp}$ are related to the reflected waves in the initial medium i, while $t_{ss,sp,ps,pp}$ are related to the transmitted waves in the final medium f.

The simulation focuses on the reflected waves. For the initially s-polarized incident beam, the Kerr signal magnitude $|\Phi_s|$ is defined as $|r_{ps}/r_{ss}| \equiv |E_{ip}^{(r)}/E_{is}^{(r)}|$ and the reflectivity is $R_s \equiv |r_{ss}| \equiv |E_{is}^{(r)}/E_{is}^{(i)}|$. For the initially p-polarized incident beam, the Kerr signal magnitude $|\Phi_p|$ is defined as $|r_{sp}/r_{pp}| \equiv |E_{is}^{(r)}/E_{ip}^{(r)}|$ and the reflectivity is $R_p \equiv |r_{pp}| \equiv |E_{ip}^{(r)}/E_{ip}^{(i)}|$. $|\Phi_{s,p}|^2$ equals the ratio of the energy of the reflected p-/s- polarized beam over the energy of reflected s-/p-polarized beam, $|\Phi_{s,p}|$ characterizes the change of the initial incident beam's polarization. $|R_{s,p}|^2$ equals the ratio of the energy of the reflected s-/p- polarized beam over the energy of the initial incident s-/p- polarized beam.

The $4\times4$ characteristic-matrix $\mathscr{M}$ can be decomposed into four $2\times2$ matrices $G$, $H$, $I$, $J$. The Matrix $G^{-1}$ and $IG^{-1}$ are related to the magneto-optic coefficients [3, 5].

$$\mathscr{M} \equiv \begin{pmatrix} G & H \\ I & J \end{pmatrix},\ G^{-1} = \begin{pmatrix} t_{ss} & t_{sp} \\ t_{ps} & t_{pp} \end{pmatrix},\ IG^{-1} = \begin{pmatrix} r_{ss} & r_{sp} \\ r_{ps} & r_{pp} \end{pmatrix} \tag{5}$$

We implement the simulation in MATLAB. The Key to simulation is to construct the characteristic-matrix $\mathscr{M}$, from which we can extract the Kerr signal strength and the reflectivity. The simulation workflow follows these three steps:

(Step *I*) Construct the $4\times4$ characteristic-matrix $\mathscr{M} = A_i^{-1}(\Pi_{m=1}^{M}A_mD_mA_m^{-1})A_f$.

(Step *II*) Extract $2\times2$ matrix $IG^{-1}$ and the magneto-optic constant $r_{ss}$, $r_{sp}$, $r_{ps}$ and $r_{pp}$ according to Eq. (5).

(Step *III*) Visualize Kerr signal magnitude $|\Phi_{s,p}|$ and reflectivity $R_{s,p}$.

In this simulation, we study the multilayer MOKE of a Fe-Cu superlattice. The setup geometry can be referred to Fig. 1, the incident plane is the y-z plane. The initial medium i is the vacuum, and the final medium f is a Cu substrate. The Cu substrate is much thicker than the superlattice, so we assumed the substrate to be infinitely thick in the simulation. On the Cu substrate there is a $\mathscr{N}$ period Fe-Cu superlattice, the superlattice is formed by stacking up the Fe film - Cu film unit for $\mathscr{N}$ times, Fe film and Cu film have the same thickness $d$. A 20Å thick Cu protective layer is placed on the top of the superlattice.

We focus on two magnetization configurations, one is magnetization parallel to the z-axis, namely polar magnetization, or POL for a shorthand; The other one is magnetization parallel to the y-axis, namely longitudinal magnetization, or LON. In the simulation, we assume that the Fe films are uniformly polarized.

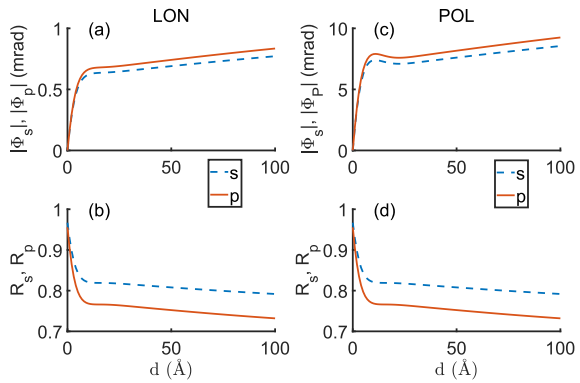


FIG. 3. Thickness dependence of Kerr signal magnitude $|\Phi_{s,p}|$ and reflectivity $R_{s,p}$. The incident angle $\theta_i = 30^\circ$ and period $\mathcal{N} = 20$, (a) and (b) are plots for LON, (c) and (d) are plots for POL.

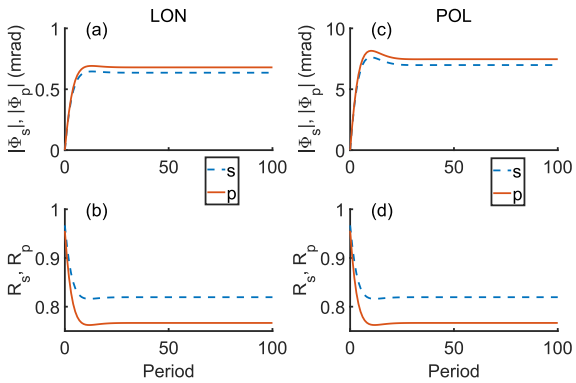


FIG. 4. Period $\mathcal{N}$ dependence of Kerr signal magnitude $|\Phi_{s,p}|$ and reflectivity $R_{s,p}$. The incident angle $\theta_i = 30^\circ$ and thickness $d = 20\text{Å}$, (a) and (b) are plots for LON, (c) and (d) are plots for POL.

A He-Ne laser with a 6328Å wavelength produces the initial incident beam. At this wavelength, based on Ref. [6], the refraction indices of Fe and Cu are $N_{Fe} = 2.87 + 3.36i$ and $N_{Cu} = 0.249 + 3.42i$. The Voigt magneto-optic constants of Fe and Cu are $Q_{Fe} = 0.0376 + 0.0066i$ and $Q_{Cu} = 0$ according to Ref. [7].

Let us first vary the thickness $d$ of the Fe film and explore the thickness dependence of the Kerr signal magnitude $|\Phi_{s,p}|$ and the reflectivity $R_{s,p}$. The period $\mathcal{N}$ is fixed as 20 and the incident angle is fixed as 30°. $|\Phi_{s,p}|$ and $R_{s,p}$ are plotted in Fig. 3.

Fig. 3 reveals some common features in the thickness dependence of $|\Phi_{s,p}|$ and $R_{s,p}$ for both LON and POL configurations. When the thickness $d$ is small ($0 < d < 5\text{Å}$), the $d$-dependence of $|\Phi_{s,p}|$ and $R_{s,p}$ is linear. At $d = 0$, only two mediums are present: the vacuum and the nonmagnetic Cu substrate (with the protective Cu layer treated as part of the Cu substrate), at this point, $|\Phi_{s,p}| = 0$, indicating that the light reflected from the Cu substrate surface does not undergo the polarization change, that is, an initially s-polarized (p-polarized) incident beam remains s-polarized (p-polarized) upon reflection. For $d > 0$, $|\Phi_s| < |\Phi_p|$. Notably, Figs. 3(b) and 3(d) demonstrate identical $d - R_s$ and $d - R_p$ relations for the LON and POL configurations, consistent with similar results reported in Ref. [3]. At $d = 0$, $R_s = R_p$, implying that the same fraction of energy from the initially s- or p- polarized incident beams is transmitted and absorbed into the Cu substrate.

A distinct difference between the LON and POL configurations emerges in the behavior of $|\Phi_{s,p}|$. For $d > 4\text{Å}$, POL exhibits a significantly stronger Kerr signal, with $|\Phi_{s,p}|$ ranging from 5 mrad to 9 mrad compared to LON, where $|\Phi_{s,p}|$ remains between 0.5 mrad and 0.8 mrad, this indicates a more pronounced polarization change between the initial incident beam and the reflected beam in the POL configuration. Additionally, in POL, as shown in Fig. 3(c), both $|\Phi_s|$ and $|\Phi_p|$ exhibit a Kerr signal hump around $d = 11\text{Å}$, while the Kerr signal hump is not observed in the LON configuration.

In the second simulation, we fix the thickness $d$ to be 20Å and the incident angle to be 30°, and vary the period $\mathcal{N}$ from 0 to 100. The period dependence of $|\Phi_{s,p}|$ and $R_{s,p}$ are displayed in Fig. 4.

There are notable similarities between the LON and POL configurations. Figs. 4(b), 4(d) are identical, indicating that the reflectivity $R_s$ (or $R_p$) share the same period $\mathcal{N}$ dependence between the LON and POL configurations. Both $R_s$ and $R_p$ exhibit a local minimum around $\mathcal{N} = 10$. The Kerr signal magnitude $|\Phi_{s,p}|$ as well as the reflectivities $R_{s,p}$ stabilize to constant values when $\mathcal{N} > 20$. At $\mathcal{N} = 0$ – corresponding to the absence of Fe film and Cu film – the values of $|\Phi_{s,p}|$ and $R_{s,p}$ match those shown in Fig. 3 for $d = 0$. For $d > 0$, it is observed that $|\Phi_s| < |\Phi_p|$ and $R_s > R_p$.

The primary difference between the LON and POL configurations lies in the magnitude of $|\Phi_{s,p}|$, POL exhibits a consistently stronger Kerr signal. When $\mathcal{N} > 3$, $|\Phi_{s,p}|$ for LON ranges from 0.5 mrad to 0.7 mrad, while $|\Phi_{s,p}|$ for POL is between 5 mrad and 8 mrad, this indicates that POL induces a more pronounced polarization change between the reflected beam and the initial incident beam. Additionally, both $|\phi_s|$ and $|\phi_p|$ in POL display a Kerr signal hump between $\mathcal{N} = 6$ and $\mathcal{N} = 20$, reaching a maximum value around $\mathcal{N} = 10$, as shown in Fig. 4(c). In contrast, LON shows only a faint Kerr signal hump in $|\Phi_p|$, observed between $\mathcal{N} = 8$ and $\mathcal{N} = 19$, as shown in Fig. 4(a).

In the last simulation, we fix the thickness $d = 20\text{Å}$ and the period $\mathcal{N} = 20$, explore the Kerr signal magnitude $|\Phi_{s,p}|$ and the reflectivity $R_{s,p}$ as the initial incident angle $\theta_i$ varies from $-90^\circ$ to $90^\circ$. The plots of $|\Phi_{s,p}|$ and $R_{s,p}$ are displayed in Fig. 5.

Some common features between the LON and POL configurations can be identified: Figs. 5(b), 5(d) are identical, implying that $R_s$ and $R_p$ do not depend on the magnetization configurations. The reflectivities $R_{s,p}$ are symmetric, $R_s$ reaches minimum at $\theta_i = 0$, while $R_p$ exhibits a local maximum at $\theta_i = 0^\circ$ and a minimum value around $\theta_i = \pm 1.3$ rad ($\pm 75^\circ$). At $\theta_i = 0^\circ$ and $\pm 90^\circ$, $R_s$ and $R_p$ coincide. Additionally, $R_p$ is consistently smaller than $R_s$. Another shared feature between the LON and POL configurations is that both $|\Phi_s|$ and $|\Phi_p|$ are symmetric and coincide at $\theta_i = 0^\circ$ and $\pm 90^\circ$. At $\theta_i = \pm 90^\circ$, the initial incident light beam in the vacuum propagates along

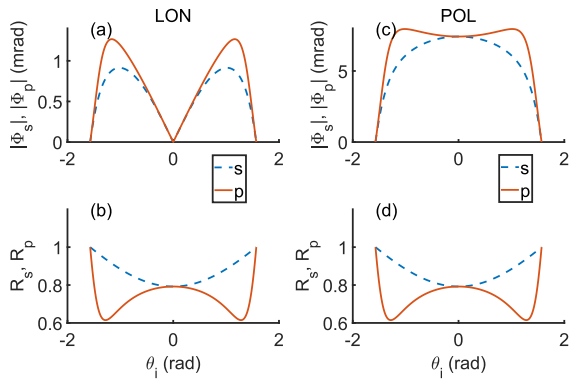


FIG. 5. Initial incident angle $\theta_i$ dependence of Kerr signal magnitude $|\Phi_{s,p}|$ and reflectivity $R_{s,p}$. The thickness $d = 20\text{Å}$ and the period $\mathcal{N} = 20$, (a) and (b) are plots for LON, (c) and (d) are plots for POL.

the y-direction and is not reflected, resulting in $|\Phi_{s,p}| = 0$ and $R_{s,p} = 1$, as shown in Fig. 5(a) – 5(d). However, the observation that $|\Phi_s| = |\Phi_p|$ at $\theta_i = 0^\circ$ requires further investigation. Overall, $|\Phi_p|$ is consistently larger than $|\Phi_s|$ in both POL and LON configurations.

The dependence of the Kerr signal magnitude $\Phi_{s,p}$ on the initial incident angle $\theta_i$ differs between the LON and POL configurations. For LON, as shown in Fig. 5(a), $|\Phi_s|$ reaches its maximum value of 0.91 mrad around $\theta_i = \pm 1.02$ rad ($\pm 58.4^\circ$), while $|\Phi_p|$ peaks at 1.27 mrad at around $\theta_i = \pm 1.16$ rad ($\pm 66.5^\circ$). At small $\theta_i$, the LON Kerr signal magnitude $|\Phi_{s,p}|$ shows a linear $\theta_i$ dependence. For POL, $|\Phi_s|$ reaches its maximum at $\theta_i = 0^\circ$, while $|\Phi_p|$ reaches its maximum at around $\theta_i = \pm 1.05$ rad ($\pm 60.2^\circ$) and a local minimum at $\theta_i = 0^\circ$. Comparing Figs. 5(a) and 5(c), the overall magnitude of $|\Phi_{s,p}|$ in POL is larger than in LON. The initial incident angle dependence of the Kerr signal magnitude is strongly influenced by the direction of the magnetization, suggesting that the variation of the Kerr signal with incident angle could be a feasible method for detecting surface magnetism.

In conclusion, we simulate the magneto-optic Kerr effect of a Fe-Cu superlattice in POL and LON configurations. For each configuration, we analyze the dependencies of Kerr signal magnitude and reflectivity on Fe-film thickness, superlattice repetition period, and the initial incident angle. Based on the simulation results, the POL displays an overall larger Kerr signal magnitude than LON. The reflectivity does not depend on the magnetization configurations, and the initially p-polarized beam has a consistently smaller reflectivity and larger Kerr signal magnitude compared to the initially s-polarized beam, the initial incident angle dependence of the Kerr signal is significantly influenced by the direction of the magnetism, which could probably be applied to detect the surface magnetism of materials.

### Appendix A: Boundary-matrix A and Propagation-matrix D

Inside the magnetic film 1, as indicated in Fig. 2(b), the boundary- matrix A and the propagation-matrix D are [4]:

$$A_1 = \begin{pmatrix} 1 & 0 & 1 & 0 \\ \frac{i}{2}\frac{\alpha_{1y}}{\alpha_{1z}}Q(\alpha_{1y}g_{1i} - 2\sin\theta\cos\phi) & \alpha_{1z} + i\alpha_{1y}\sin\theta\cos\phi Q & -\frac{i}{2}\frac{\alpha_{1y}}{\alpha_{1z}}Q(\alpha_{1y}g_{1r} - 2\sin\theta\cos\phi) & -\alpha_{1z} + i\alpha_{1y}\sin\theta\cos\phi Q \\ \frac{i}{2}N_1 g_{1i}Q & -N_1 & \frac{i}{2}N_1 g_{1r}Q & -N_1 \\ N_1\alpha_{1z} & \frac{iN_1}{2\alpha_{1z}}g_{1i}Q & -N_1\alpha_{1z} & -\frac{iN_1}{2\alpha_{1z}}g_{1r}Q \end{pmatrix} \tag{A1}$$

$$D_1 = \begin{pmatrix} U_1 & U_1\delta_{1i} & 0 & 0 \\ -U_1\delta_{1i} & U_1 & 0 & 0 \\ 0 & 0 & U_1^{-1} & -U_1^{-1}\delta_{1r} \\ 0 & 0 & U_1^{-1}\delta_{1r} & U_1^{-1} \end{pmatrix} \tag{A2}$$

Where $\alpha_{1y} = N_i\sin\theta_i/N_1$, $\alpha_{1z} = \sqrt{1-\alpha_{1y}^2}$, $\alpha_{1z} = \sqrt{1-\alpha_{1y}^2}$, $\alpha_{1z} = \sqrt{1-\alpha_{1y}^2}$. $g_{1i} = \cos\theta\alpha_{1z} + \sin\theta\sin\phi\alpha_{1y}$, $g_{1r} = -\cos\theta\alpha_{1z} + \sin\theta\sin\phi\alpha_{1y}$. $U_1 = \exp(-i\frac{2\pi}{\lambda}N_1 d_1\alpha_z)$, $\delta_{1i} = \frac{\pi}{\lambda}N_1 d_1\frac{Q}{\alpha_{1z}}g_{1i}$, $\delta_{1r} = \frac{\pi}{\lambda}N_1 d_1\frac{Q}{\alpha_{1z}}g_{1r}$. $\theta$ and $\phi$ are the polar and azimuthal angles of the magnetization. $\lambda$ is the vacuum wavelength of the light source.

The incident angle $\theta_1^{(\bar{1},\bar{2},\bar{3},\bar{4})}$ of modes $\bar{1}$, $\bar{2}$, $\bar{3}$ and $\bar{4}$ are: $\alpha_{1y}^{(\bar{1},\bar{2})} = \sin\theta_1^{(\bar{1},\bar{2})} = \alpha_{1y}(1 \mp \frac{1}{2}g_{1i}Q)$, $\alpha_{1y}^{(\bar{3},\bar{4})} = \sin\theta_1^{(\bar{3},\bar{4})} = \alpha_{1z}(1 \mp \frac{1}{2}g_{1r}Q)$, $\alpha_{1z}^{(\bar{1},\bar{2})} = \alpha_{1z}(1 \pm \frac{1}{2}g_{1i}Q)$, $\alpha_{1z}^{(\bar{3},\bar{4})} = -\alpha_{1z}(1 \pm \frac{1}{2}\frac{\alpha_{1y}^2}{\alpha_{1z}^2}g_{1r}Q)$. $\theta_i$ and $N_i$ are the initial incident angle and the refraction index in the initial medium i.

[1] D. Kim, Y. W. Oh, and J. U. K. *et al*, Nat Commun **11**, 5937 (2020).
[2] W. Kuch, *Magnetic microscopy of layered structures* (Berlin: Springer, 2015).
[3] J. Zak, E. Moog, C. Liu, and S. Bader, Journal of Magnetism and Magnetic Materials **89(1-2)**, 107 (1990).
[4] J. Zak, E. Moog, C. Liu, and S. Bader, Phys. Rev. B **43(8)**, 6423 (1991).
[5] Z. Q. Qiu and S. D. Bader, Review of Scientific Instruments **71(3)**, 1243 (2000).
[6] R. C. Weast, *CRC handbook of chemistry and physics* (CRC Press, 1986).
[7] G. S. Krinchik and V. A. Artemev, Sov. Phys. JETP **26**, 1080 (1986).